Evidence for thermal mechanisms in laser-induced femtosecond spin dynamics

U. Atxitia and O. Chubykalo-Fesenko
Instituto de Ciencia de Materiales de Madrid, CSIC, Cantoblanco, 28049 Madrid, Spain

J. Walowski, A. Mann, and M. Münzenberg
I. und IV. Physikalisches Institut, Universität Göttingen, 37077 Göttingen, Germany

(Received 19 December 2009; revised manuscript received 11 March 2010; published 4 May 2010)

Recent pump-probe experiments using powerful femtosecond lasers and x-ray magnetic circular dichroism have opened a debate on the origin of the magnetization modification on the femtosecond time scale. We show a quantitative agreement between femtosecond optical pump-probe experiments and thermal micromagnetic modeling in nickel, which reveals a predominant thermal demagnetization mechanism. Magnetic fluctuations are introduced in the system as spin-flip processes due to scattering mechanisms in the electron system. In our model the Landau-Lifshitz-Bloch equation for a macrospin (containing the statistically averaged magnetic fluctuations) is coupled to the electronic temperature of the two-temperature model whose parameters are extracted from the measured reflectivity. We show that the demagnetization and the magnetization recovery time slow down as the laser pump fluence is increased and identify the longitudinal relaxation as a key factor for the observed behavior.

DOI: 10.1103/PhysRevB.81.174401 PACS number(s): 75.40.Gb, 75.70.−i, 78.47.−p

I. INTRODUCTION

The implementation of future magnetic recording and spintronic devices requires well-funded knowledge of the limits of spin manipulation. Pump-probe experiments with powerful femtosecond lasers have pushed these limits down to the femtosecond time scale in the past decade.[1–11] These experiments have attracted many researchers with the aim of understanding both the fundamental mechanisms and control of the magnetic properties of materials on the femtosecond time scale. However, even for the simplest itinerant ferromagnets, such as Ni, the underlying elementary mechanisms leading to the macroscopic demagnetization on the femtosecond time scale have not yet been identified. The challenge lies in the complexity of a parallel, dynamic treatment of photons, electrons, phonons, and magnetic correlations of the spin system on different length and time scales.

A starting point for modeling the evolution of the highly nonequilibric situation can be to follow the flow of angular momentum and/or the flow of energy. Although the role of angular momentum transfer is undoubtedly important and is a fundamental question in the femtosecond spin dynamics, little understanding has been achieved so far. Theoretical approaches beyond Born-Oppenheimer approximation to trace ultrafast angular momentum transfer are out of reach and novel experimental approaches have to be developed. However, estimations suggest that the amount of direct angular momentum transfer from photons to spins is negligible.[12] In addition recent experiments using x-ray absorption spectroscopy[5] by separating the spin and orbit magnetic moment could exclude an ultrafast transfer of magnetic moment from the spin to the orbital channel on a femtosecond time scale. Several mechanisms of how light could couple directly to the spin system to describe femtosecond spin dynamics have been put forward: the excitation of nonmagnetic states mediated by the enhanced spin-orbit interaction,[13] the inverse Faraday[14] or the Barnet effect.[15] At the moment, no proof that the two latter effects are of strong relevance for the ultrafast magnetization dynamics in Ni has been presented, reflected in an absence of a strong sensitivity to the pump-pulse polarization.[12] Thus the major role in the conservation of angular momentum will be taken by the lattice, mediated by the spin-orbit interaction.

Alternatively a "thermal" nondeterministic description of the femtosecond magnetization dynamics in the itinerant ferromagnets[1,3,16–18] has been proposed describing the flow of energy. Within these approaches, it is assumed that the excited state is a statistical ensemble of many electronic excitations, based on the fact that the photons of a femtosecond laser, focused on a metal, pass the energy to the subsystems of electrons where phonons and spins are involved in its subsequent redistribution. The photons are absorbed by electrons close to the Fermi level, leading to a nonequilibrium electron distribution that thermalizes within several femtoseconds. In the so-called two-temperature ($2T$) model,[19–21] energy dissipation in the system is introduced by including rate equations, attributing temperatures to electrons and lattice. The thermal model assumes that stochastic spin-flip processes are driven by the increased electron temperature. In this line a thermal formalism based on the stochastic Landau-Lifshitz-Gilbert equation was developed to model the subpicosecond spin dynamics within an atomistic discrete Heisenberg model by Kazantseva *et al.*[16] Within this model, as well as in a micromagnetic approach,[22] the presence of terahertz (THz) high-energy spin waves was demonstrated. These studies reveal the necessity of including the intrinsic magnetic fluctuations of the excited spin system to describe the femtosecond demagnetization experiments. A similar model allowing one of the first quantitative comparisons has been published recently.[23] In this model the spin fluctuations have been introduced by a mean-field Weiss model and incorporating thermal statistics with spin $S=1/2$.

In an elegant coarse-grained description the fluctuations of the spin subsystem are included in the *thermal macrospin*, schematically depicted in Fig. 1. The laser pulse excites the spin system via the electron system. This leads to spin sys-

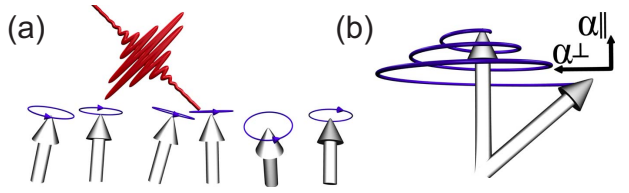

FIG. 1. (Color online) Schematics of the thermal model. The laser deposits energy on the spin system leading to the excitation of THz spin waves (left). The resulting "macrospin" (right) experiences two relaxations: longitudinal and transverse damping $\alpha_{\parallel}$ and $\alpha_{\perp}$.

tem disordering on the time scale of femtoseconds that reduces the total magnetization in average (reduction in the longitudinal magnetization component in the macrospin approximation). The effect can be described as "heating" due to the energy input from the other systems. The high-energy spin fluctuations are statistically averaged and mirrored in temperature-dependent parameters. This novel micromagnetic approach to describe femtosecond dynamics is based on the Landau-Lifshitz-Bloch (LLB) equation[17,24] and will be used in the following. It has the advantage that, in addition to a pure statistical description of thermal spin ensembles, it is a real dynamic equation.

The thermal excitations which disorder the spin system have to arise from a microscopic spin-flip process, acting on a femtosecond time scale. Presently there is an active debate on the possible candidates for the microscopic spin-flip processes leading to femtosecond demagnetization which we cannot resolve in our experiments. However, we will present our view on the current understanding: the elementary scattering events in a quantum description can be divided into two processes that are seen to be most relevant, depicted schematically in Fig. 2. The first candidate is the Elliott-Yafet[25–27] process. As we have discussed earlier,[11] it makes use of the fact that due to spin-orbit interaction the spin of the electron is not a good quantum number anymore and, as a consequence, intermixes the spin channels at some high-symmetry points of the band structure. If the electrons, heavily excited by the energy input of the intense femtosecond laser pulse, are scattered into these spin hot spots in the Fermi surface (by defects, phonon-scattering events, etc.), the final state has a certain probability to be of opposite spin

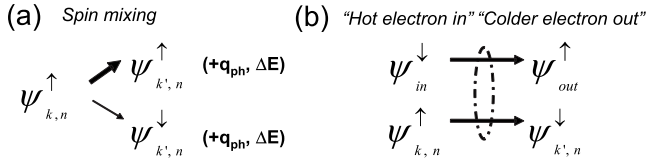

FIG. 2. Schematics of the spin-flip processes. (a) Elliott-Yafet process of an electron-scattering event with a phonon to an unoccupied intraband band state is depicted. The spin-orbit interaction intermixes the spin channels in some points of the band structure. In the final state a certain probability of a reversed spin is given. The phonon takes energy and momentum from the electron system. (b) Exchange scattering of a hot electron which in effect exchanges the spin orientation of the hot electron and the locally remaining electron at lower energy.

direction.[28] A spin mixing can be calculated and is a factor of 20 higher in Ni than in Cu, which explains the observed time scales in femtosecond spin dynamics.[26] This first elementary scattering mechanism reduces the total magnetization. The second process which is currently discussed is the electron-electron scattering mediated by exchange interaction.[29,30] It is suggested to be a dominant spin-scattering contribution at higher energies.[29] An electron at around the Fermi level is excited by an incoming hot electron of opposite spin direction. While the hot electron relaxes to an unoccupied state at the Fermi level, the second electron takes up the energy of the hot electron. After the scattering process both have exchanged their spin orientation, a process well known from spin-polarized electron energy-loss spectroscopy.[31] In this second case, as long as the hot electron remains in the ferromagnet, the total magnetization is not reduced, as can be seen in Fig. 2. However in both cases an electron with opposite spin remains at around the Fermi level. The excited spin state will not be stable in its environment and will further decay into spin excitations of lower energy.[22] The subsequent relaxation path of this Stoner-type excitation can be pictured as follows: from the localized Stoner process, described in a Hubbard-type model band, a propagator can be constructed equivalent to a delocalized magnon and both can be transformed into each other.[32] This results into multiple interaction channels and allows different relaxation paths in a broad energy range where both the spin-wave dispersion and the single-particle excitation spectrum overlap (for energies larger than $\Delta_{ex}-E_F$), suggesting an important role in the spin-relaxation process. Strong interactions were first discussed in connection with neutron-scattering experiments in 1970s, where the spin-wave excitation branches for high-energy spin waves in the transition-metal ferromagnets are broadened heavily. Approaching the Brillouin-zone boundary they finally disappear.[33] These effects have been theoretically described in the dynamic susceptibility of the spin system later.[34] We want to stress explicitly that the density of spin excitations in femtosecond demagnetization experiments is very high: the averaged magnetization is reduced to a level approaching half the magnetic moment per atom. In contrast to standard magnetization dynamics with small excitation amplitudes, this opens up new relaxation channels not observed before. In other words, to describe femtosecond magnetization dynamics correctly the single electron picture intrinsic to the Elliott-Yafet model has to be mapped to a correlated ferromagnetic material with collective spin excitations in a highly nonequilibrium situation. It should be noted that the electronic nature of the spin excitation in the Stoner picture cannot be regarded in the following as part of a micromagnetic equation. However, the subsequent relaxation into high-energy spin-wave excitations thereafter will be mirrored in the longitudinal relaxation included in the macrospin approximation at a later stage and can be followed in the thermal macrospin model.

In our LLB macrospin approach, the microscopic spin-flip process is parameterized by the coupling parameter λ between the spin and the electron system. Here we use the fact that spin-orbit interaction intermixes the spin channels and allows spin-flip processes in principle. The thermal macrospin is also advantageous because of a reduced computa-

tional expense compared to the atomistic calculations. Note that for an infinite spin $S \rightarrow \infty$ the LLB approach coincides with that of the discrete Heisenberg model. At the same time this approach is more general since the restriction of the classical spin is removed and characteristics of itinerant ferromagnets, their quantum character and scattering mechanisms can be implemented in extension of the model in the future. Although the thermal ideas have been expressed previously in several articles, we present a quantitative comparison between the experiment and model for the ultrafast magnetization dynamics in Ni for a set of different excitation powers and thin-film thickness using the LLB equation. The excellent agreement between experiment and model proves that the ultrafast demagnetization in Ni can be modeled assuming a purely thermal origin.

II. EXPERIMENT

Our experiment was performed on 10–40-nm-thick ferromagnetic Ni films deposited on a Si(100) substrate using electron-beam evaporation in ultrahigh vacuum (5×10^{-10} mbar). A femtosecond pump-probe experiment was used to determine the reflectivity $R(\tau)$ and the Kerr rotation $\theta_K(\tau)$ as a function of the probe pulse delay τ (Refs. 2 and 22) for uncapped films immediately after sample preparation. The exciting pump-pulse fluence was varied from 10 to 50 mJ/cm^2 per pulse (80 fs, $\lambda = 800$ nm), calculated from the area determined from the half width of the Gaussian pump beam intensity profile (60 μm). A static field was applied in plane to saturate the sample. The Kerr rotation $\theta_K(\tau)$ is defined in the following as the asymmetric part of the signal, $\theta_{K,-}(\tau) = \frac{1}{2}[\theta_K(\tau, M) - \theta_K(\tau, -M)]$ changing with the field direction and mirroring predominantly the magnetization change. The symmetric part $\theta_{K,+}(\tau) = \frac{1}{2}[\theta_K(\tau, M) + \theta_K(\tau, -M)]$ mirrors the reflectivity change $R(\tau)$. However the reflectivity change $R(\tau)$ was determined separately by a differential measurement method of the direct sample reflectivity for p-polarized probe pulses. The optical penetration depth for Ni is $\lambda_{opt} \approx 14$ nm and absorbed laser power decays as a function of the distance from the surface. Consequently, the resulting demagnetization for various pump fluences F for Ni thicknesses from 10, 15, 20, and 40 nm can be rescaled to the absorbed fluence per Ni layer S, see Fig. 3. Therefore in the following we will restrict our modeling to the 15 nm Ni film without losing generality.

The data of the delayed reflectivity $R(\tau)$ for various pump fluences are presented in Fig. 4 and show a contribution mirroring the electron dynamics with a steep peak like increase that equilibrates on a constant slope plus oscillations with a main period of about 7 ps (see supplementary materials for nonshifted presentation). They originate from the coherent excitation of a shockwave (sound velocity $\nu_{Ni} = 5400$ m/s). In the case of a film thickness in the range of $t_{Ni} \sim t_{opt,800\ nm}$ a standing shock wave forms with the wave vector $k = \pi / t_{Ni}$.[35] For a threshold fluence above 30 mJ/cm^2 the strong coherent stress wave excitations appear to have an incoherent counterpart (lattice heating and thermal expansion) owing to an effect on the reflectivity. The transient reflectivity $R(\tau)$ will be taken as an independent input to extract the relevant parameters for the modeling of the electron temperature $T_e(t)$ later.

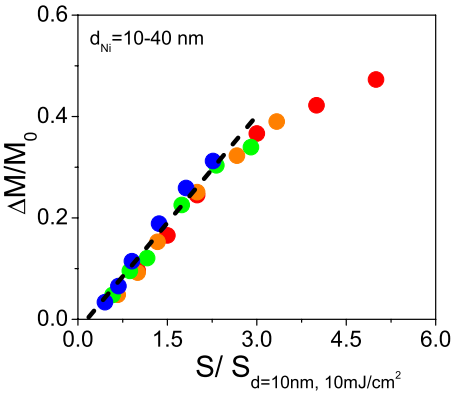

FIG. 3. (Color online) The results of the femtosecond demagnetization for pump fluence $F = 10\text{-}50$ mJ/cm^2 and for Ni thicknesses of 10, 15, 20, and 40 nm rescaled to the absorbed fluence per Ni layer S.

III. MODEL

The LLB equation used to describe the magnetization dynamics including thermal effects has been derived for the dynamic motion of a statistically averaged thermal spin ensemble **m** by Garanin.[36] In a classical case starting from a stochastic Landau-Lifshitz-Gilbert equation and using the mean-field approximation (MFA), Garanin derives a macroscopic equation including spin fluctuations driven by a heat bath at temperature T. The equation allows a similar formulation for the quantum case[36] incorporating the microscopic scattering mechanisms. In a comparative study with atomistic simulations, the macrospin LLB equation has been shown to be a valid micromagnetic dynamic extension of the Landau-Lifshitz-Gilbert equation even above T_c, namely, incorporating the effect that, approaching the phase transition, the magnetization amplitude is not constant and that the damping of the precessing magnetization **m** is enhanced.[37] In ultrafast demagnetization experiments where the electron system is not in thermal equilibrium with the spin system, the rates of the demagnetization and remagnetization process calculated from the LLB model qualitatively agree with the experiment.[17,24] The main assumption of these thermal models is that the hot electrons provide a heat bath for the spin dynamics.[16] This is a reasonable assumption: in a good approximation for a ferromagnetic transition metal microscopically the spin system is dominantly coupled to the electronic temperature.[10] In the following the heat bath temperature T is set to $T = T_e(t)$, the electronic temperature, driving the magnetic fluctuations and the weaker spin-lattice interaction will be neglected on the ultrafast time scale. It will be shown in the following in how far a quantitative description of the magnetization dynamics using the LLB equation is possible.

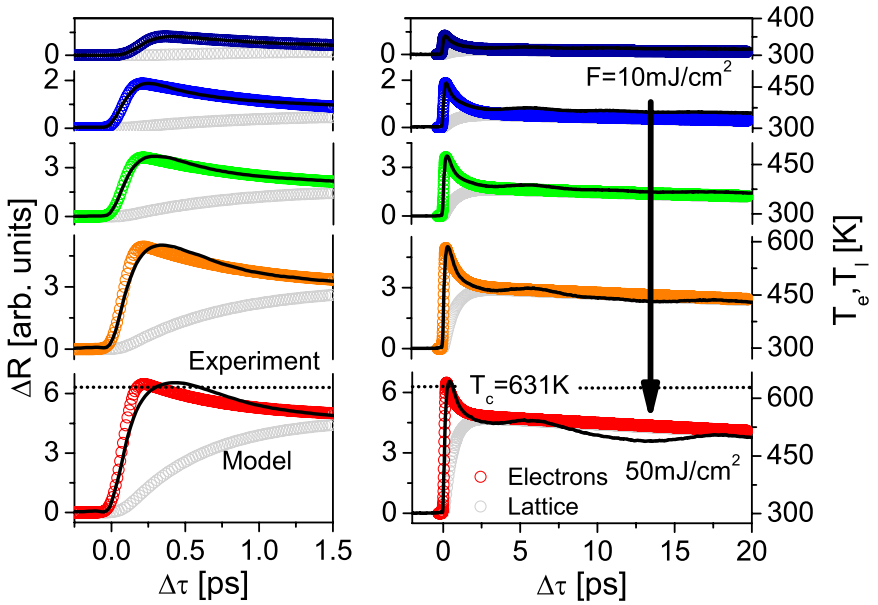

FIG. 4. (Color online) Response after femtosecond laser excitation revealing the dynamics of the heated electrons, coherent stress waves, and incoherent lattice excitations at various pump fluences F contributing to the transient reflectivity for a 15 nm Ni thin film (solid lines). The relaxation rates allow to extract the parameters for the integration of the $2T$ model from the normalized curves. Therefore the electron temperatures T_e (colored symbols) and lattice temperature T_l (gray symbols) are derived as described in the text. Note that a different linear scale relating ΔR and T_e was used to present the data for different fluences F (Table II, supplementary materials). The same data are plotted on the long time scale (right) and subpicosecond time scale for details (left).

We write the LLB equation as follows:

$$\dot{\mathbf{m}} = \gamma[\mathbf{m} \times \mathbf{H}_{\text{eff}}] + \frac{\gamma\alpha_{\parallel}}{m^2}[\mathbf{m} \cdot \mathbf{H}_{\text{eff}}]\mathbf{m} - \frac{\gamma\alpha_{\perp}}{m^2}[\mathbf{m} \times (\mathbf{m} \times \mathbf{H}_{\text{eff}})], \tag{1}$$

where $\mathbf{m}=\mathbf{M}/M_s(T=0)$, γ is the gyromagnetic ratio, $\alpha_{\parallel}$ and $\alpha_{\perp}$ are dimensionless longitudinal and transverse damping parameters given by $\alpha_{\parallel}=2\lambda T/3T_c$, $\alpha_{\perp}=\lambda[1-T/3T_c]$ for $T<T_c$ and $\alpha_{\perp}=\alpha_{\parallel}$ for $T>T_c$. λ determines the coupling strength of the spins to the electron heat bath $T=T_e(t)$. In the quantum description the coupling parameter λ contains the matrix elements representing the scattering events and, thus, is proportional to the spin-flip rate due to the interaction with the environment.

The effective field $\mathbf{H}_{\text{eff}}$ is given by

$$\mathbf{H}_{\text{eff}} = \mathbf{H} + \mathbf{H}_A + \begin{cases} \dfrac{1}{2\tilde{\chi}_{\parallel}}\left(1 - \dfrac{m^2}{m_e^2}\right)\mathbf{m} & T \lesssim T_c \\ -\dfrac{1}{\tilde{\chi}_{\parallel}}\left[1 - \dfrac{3T_c}{5(T-T_c)}m^2\right]\mathbf{m} & T \gtrsim T_c. \end{cases} \tag{2}$$

In our model the temperature-dependent equilibrium magnetization m_e and longitudinal susceptibility $\tilde{\chi}_{\parallel}$ were determined from MFA by adjusting the Curie temperature value to the experimental one $T_c=631$ K. In a more rigorous multiscale description,[17] they can be evaluated directly from the spin Hamiltonian, parametrized from the electronic-structure calculations, or considered as an experimental input. Here the temperature-dependent equilibrium magnetization m_e is derived for infinite spin $S\to\infty$ using the Langevin function.[24] We use the following parameters for Ni: the saturation magnetization $M_s=500$ emu/cm^3 (at $T=0$ K), the applied field was $\mathbf{H}=1500\mathbf{e}_x$ Oe. The easy-plane anisotropy, defined by magnetostatic interactions for the thin-film geometry, is given by $\mathbf{H}_A=4\pi M_s$ $(m_x\mathbf{e}_x+m_y\mathbf{e}_y)$. The magnetocrystalline anisotropy is neglected. Finally the damping parameter for the Ni films is $\alpha_{\perp}=0.04$ at $T=300$ K as experimentally determined.[22] The intrinsic coupling parameter $\lambda=0.045$ directly follows from the transverse relaxation $\alpha_{\perp}$. Therefore all parameters that enter into the equation of motion [Eq. (1)], besides the electron temperature T_e, have been determined independently from the experiment.

To determine the electron temperature $T_e(t)$ we analyze the transient experimental time-resolved reflectivity shown in Fig. 4. To calculate the electronic temperature $T_e(t)$ within a two-temperature ($2T$) model (symbols), the relevant parameters are extracted from the decay rates of the measured reflectivity (solid lines). The assumption needed here that in first approximation the reflectivity is defined by the electron temperature $R(t)\propto T_e(t)$, which is only valid on a small range with limitations.[20] The electron temperature $T_e(t)$ is coupled to the lattice temperature T_l within the $2T$ model[19] in the form of two differential equations,

$$C_e\frac{dT_e}{dt} = -G_{el}(T_e - T_l) + P(t) - C_e\frac{(T_e - T_{\text{room}})}{\tau_{th}},$$

$$C_l \frac{dT_l}{dt} = G_{el}(T_e - T_l), \tag{3}$$

Here C_e and C_l are the specific heats of the electrons and the lattice and G_{el} is an electron-phonon coupling constant which determine the rate of the energy exchange between the electrons and the lattice,[21] and τ_{th} is the heat diffusion time. In addition the following assumption enter into to the numerical solution: the electron specific heat should strongly depend on T_e due to variation in the density of states of Ni around the Fermi level with temperature; here we assume a simplification $C_e = \gamma_e T_e$ and $\gamma_e = 3 \times 10^3$ J m^{-3} K^{-2}. The lattice specific heat at low pump fluences is $C_l = C(300\ \mathrm{K}) - C_e(300\ \mathrm{K}) = 3.1 \times 10^6$ J m^{-3} K^{-1}, where $C(300\ \mathrm{K}) = 4 \times 10^6$ J m^{-3} K^{-1} is the experimental total specific heat of Ni.[38] The remaining parameters of the model were obtained by the fitting of the reflectivity for all data from Fig. 4 using the following procedure (see details in the supplementary material section:[18,44] from the low-fluence reflectivity curve the scattering rate G_{el} was determined by the first decay rate, i.e., the electron-phonon equilibration time τ_{ep}. This procedure gives $G_{el} \approx 10 \times 10^{17}$ W m^{-3} K^{-1}, consistent with similar values reported for Ni earlier.[39] The heat diffusion time of $\tau_{th} \approx 50$ ps was determined by the slow decay on the long term behavior, related to the time needed to equilibrate the heated film with the ambient temperature. Next both the reflectivity and the electron temperature curves were normalized to $\Delta R^{\max}$ and $T_e^{\max}$, respectively. At high pump fluency, the fitting of the $2T$ model to the reflectivity data shows that as the energy deposited increases, a decrease in the ratio $T_e^{\max}/T_l^{\max}$ is observed, related to the ratio of C_l/γ_e. This decrease may contain different contributions not included in our simplistic model, such as (i) nonlinear temperature dependence of the specific heat C_e, (ii) fluence dependence of the energy dissipation mechanisms G_{el}, or (iii) dependence of the reflectivity data on T_l at high pump fluencies.[35] The behavior was taken into account by considering that the lattice specific heat is a function of the pump fluency decreasing from the value above (at the lowest pump fluence) down to $C_l = 1.0 \times 10^6$ J m^{-3} K^{-1} at the highest pump fluence. This choice remains at this point arbitrary but will have no impact on our final analysis since the numerical model is adapted to the experimental electron temperature. Alternatively, we could have used the adjustment of the γ_e value, as in Ref. 23, which would produce a similar effect. Finally, the absolute-temperature variation has to be calculated, determined by the Gaussian source term $P(t)$ which describes the laser power density absorbed in the material. It is proportional to the Fluence $F(t)$. The proportionality factor is difficult to determine in praxis because the absorption of substrate and interfaces is typically found too large. It is determined from the boundary condition of the numerical calculation: the temperature of the electron system T_e is set to the temperature of the spin system T_s for long time scales [determined from the demagnetization via $m_e(T_s) = (M_{0,300\ \mathrm{K}} - \Delta M_{20\ \mathrm{ps}})/M_{0,0\ \mathrm{K}}$].[40] The resulting proportionality factor is independent on the laser pump fluence.

The parameterization of the $2T$ model allows now its integration for all fluences to determine the absolute temperature T_e. The results are given in Fig. 4, overlayed to the reflectivity data. The scaling factor, calculated to scale the normalized data to the model, is different for all fluences and systematically increasing by a factor of 2. Here it is used to present the data only for direct comparison, however it points to a more complex dependence in between ΔR and T_e and limits the application of a simple linear scaling. We want to note that reducing the parameters to a minimum number and keeping as many parameters the same for the fit for all fluence data, a reasonable agreement is found. However more advanced models that include further parameters, as the electron-electron equilibration time τ_{ee} (Ref. 35) related to the steepness of the rising edge, can achieve a better description of the data. For the highest pump fluence the electron temperature exceeds the Curie temperature T_c while the lattice temperature stays well below that value.

As a central result, finally we directly calculate the femtosecond magnetization dynamics in the LLB model by coupling Eq. (1) and the integration of the rate equations, Eq. (3), taking the input temperature $T = T_e(t)$ for the heat bath. The results are presented in Fig. 5 (symbols) in direct comparison with the experimental data from the time-resolved Kerr effect $\Delta\theta_K$ normalized to the saturation value $\Delta\theta_{K,0}$ for negative delay (solid lines), equal to the magnetization $M_x/M_{x,0}$ for time scales >100 fs [$M_{x,0}$ room-temperature value ($M_{0,300\ \mathrm{K}}$), see supplementary materials for nonshifted presentation]. Characteristic effects as the double exponential remagnetization described in our earlier work are reproduced in detail.[22] Moreover the modeled data describe the experimental data in their absolute value and in their detailed slope and predicts the correct time scales. Let us focus on a very prominent feature: as the pump fluence is raised, the restoration to the original value of the magnetization slows down dramatically. It takes more than >20 ps for a demagnetization value of $0.6M_s$. For a quantitative comparison, the results of the integration (modeled data) and experimental data of Fig. 5 are analyzed using the analytic solution for the three-temperature model (including the spin temperature) given by Dalla Longa *et al.*[11,12] extended by a second remagnetization time $\tau_{M,re}$,

$$-\frac{\Delta M_x(t)}{M_{0,x}} = \left\{ \left[A_1 F(\tau_0, t) - \frac{(A_2\tau_E - A_1\tau_M)}{\tau_E - \tau_M} e^{-t/\tau_M} - \frac{\tau_E(A_1 - A_2)}{\tau_E - \tau_M} e^{-t/\tau_E} - A_3 e^{-t/\tau_{M,re}} \right] \Theta(t) \right\} * G(t). \tag{4}$$

Here $*G(t)$ represents the convolution product with the Gaussian laser-pulse profile, $\Theta(t)$ is the step function, and A_i are the fitting constants. The results are presented in Table I for direct comparison. Three time scales characterize the magnetization dynamics: the demagnetization time τ_M and the remagnetization times τ_E and $\tau_{M,re}$. We observe a slowing down of all magnetization times τ_M, τ_E, and $\tau_{M,re}$ as a function of laser pump fluence. The demagnetization time τ_M is increased by about a factor of 2. More dramatic is the effect on τ_E and $\tau_{M,re}$. A strong increase is observed. As a result, the recovery time of the magnetization τ_E and the reflectivity

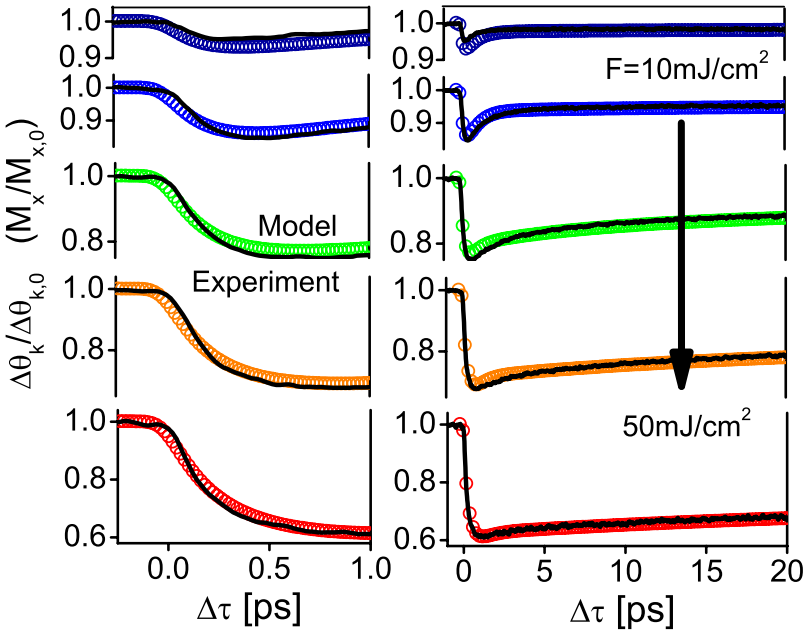

FIG. 5. (Color online) Femtosecond magnetization dynamics in the thermal macrospin model by the numerical integration (symbols) and the experimental time resolved magnetization $\Delta\theta_K/\Delta\theta_{K,0}$ (solid lines). Both are directly compared on an absolute scale for various laser pump fluences F for a 15 nm Ni film. The same data are plotted on the long time scale (right) and subpicosecond time scale for details (left).

(electron-phonon equilibration time), $\tau_{ep} \simeq 0.4-0.5$ ps, have different magnitudes. The appearance of a slowing down for high fluences is a very general phenomena. It was observed in the recovery time for Ni previously[22] and also reported for the demagnetization time for Fe and Co.[6,9] It is one of the immediate consequence of the second term in the LLB equation: it determines the rate at which the spin system disorders at a given temperature and mirrors the appearance of short-wavelength spin excitations at THz frequency, the critical slowing down.[41] Fluctuations at all length scales appear at high temperatures and result in a large dynamic longitudinal susceptibility, inversely proportional to the strength of exchange interactions ($\chi_\parallel \propto J^{-1}$) and diverging at T_c.[36,37] Thus at given pump fluency different demagnetization rates are achieved for materials with different strength of exchange interactions J. Additionally, the magnetization relaxation rate $\tau_\parallel$ is inversely proportional to the intrinsic coupling-to-the-bath parameter λ, i.e., to the scattering rate.[10,37] Both directly lead to the classification of fast and slow materials introduced recently by Koopmans.[23] Therefore one concludes that during the laser-induced demagnetization the electron temperature is changed on the time scale faster than the longitudinal relaxation time of ≈ 0.1-1 ps. Consequently, the spin system cannot follow the electron temperature. The magnetic response is delayed by the slowing down of the longitudinal relaxation, evident in a slower demagnetization (τ_M) and magnetization recovery times ($\tau_E, \tau_{M,re}$). The first experimental and theoretical approaches for FePt and CoPt attributed the slowing down of the magnetization recovery τ_E to a total magnetic correlation loss at high pump fluences.[16] In contrast to this, here even for the highest pump fluence of 50 mJ/cm^2 per pulse, the absolute measurements of the dynamic Kerr effect reveal a reduction in the magnetization of $0.6M_{0,300\ \mathrm{K}}$ within the film depth probed. This is not sufficient to produce a magnetization correlation loss. Our analysis of the reflectivity data reveals that the relative balance between the energy put into the lattice and electron system is different for high fluency compared to low fluency, mirrored

TABLE I. Direct comparison of the demagnetization time τ_M and magnetization recovery times from a two-exponential fit τ_E and $\tau_{M,re}$. Note that τ_E can differ from the electron-phonon equilibration τ_{ep} by its magnetic contribution.

	Time-resolved magneto-optic Kerr effect			LLB model		
Fluence (mJ/cm^2)	τ_M (fs)	τ_E (ps)	$\tau_{M_{re}}$ (ps)	τ_M (fs)	τ_E (ps)	$\tau_{M_{re}}$ (ps)
10	70(10)	0.70(2)		160(15)	1.18(2)	
20	101(10)	1.85(2)		175(15)	1.48(3)	
30	160(10)	2.23(4)	18.4(3)	185(15)	1.45(2)	18.55(7)
40	178(10)	3.2(1)	39(1)	215(15)	1.03(1)	26.99(6)
50	193(15)	3.7(4)	58(5)	250(10)	1.15(1)	38.51(6)

by the ratio between maximum electron and lattice temperatures (Fig. 4). We capture as an important result that only the full description of the longitudinal relaxation, mirroring the magnetic correlations of the spin system, and the cooling dynamics of the lattice and electrons together leads to the correct description of the characteristic slowing down of the magnetization recovery.

In the last part we want to discuss possible limitations. They can appear at very short time scales, where the electronic nature of the Stoner excitation may dominate the dynamics (<100 fs) and our value of the demagnetization time τ_M is consistently found too large. On the other hand also the approximation used for the thermal averaged spin distribution function, given by the Langevin function for the infinite spin $S \rightarrow \infty$, may have some limited validity. However in principle the LLB equation has no limitations and more general formulation of the LLB equation can be used to improve this imprecise description in the future.

IV. CONCLUSIONS

In conclusion, the full simulation using the thermal macrospin model reveals the thermal demagnetization mechanism in Ni mediated by thermalized hot electrons. The theoretical model allows us to identify the longitudinal relaxation as a limiting factor for the demagnetization rates, a general phenomenon which is present in all ferromagnetic materials. Therefore it is suitable for all other ferromagnets where the high-temperature dynamics of the itinerant electrons can similarly be described by a heat bath description. The longitudinal relaxation depends thereby also on the coupling strength between electron and spin system given by the coupling parameter λ. The latter means that the magnitude of the demagnetization rate strongly depends on the microscopic coupling mechanisms. λ contains the information of the microscopic spin-flip mechanism acting on femtosecond time scale, either the Elliott-Yafet scattering or the exchange scattering. Probably both mechanisms play an important role and their contribution on different time scales needs to be determined by future experiments and theory. The agreement between the experimental data and our modeled theoretical data relies very sensitively on the strength of the coupling parameter, taken as temperature independent $\lambda=0.045$ throughout the paper equal to the room-temperature value. The most successful recent calculations of damping rates in transition metals within the first-principle approach are based on the spin-orbit torque correlation functions and thus, the results depend strongly on the spin-orbit coupling and have a complicated temperature dependence.[42,43] The fact that the experimental τ_M deviates and is slightly faster than the modeling results, could suggest the possibility of an increase in λ with electron temperature for the excited ferromagnet.

On the other hand the nevertheless remarkable good agreement between measured and modeling data has been obtained using the intrinsic coupling parameter $\lambda=0.045$ determined from the experimental value of damping parameter $\alpha_\perp$. Therefore we can conclude that for Ni, in contrast to our earlier findings for rare-earth doped Permalloy films,[11] the same spin-scattering mechanism dominates the spin relaxation on long (100 ps) and femtosecond time scales. For future experiments on different ferromagnets we suggest using a multiexperimental approach as demonstrated: with varied pump fluence and film thickness, and measuring the reflectivity at the same time. This will reduce unknown parameters in the analysis to determine the electron temperature as input independent from the magnetization dynamics and come closer to the nature of the elementary spin-scattering mechanism. Decisive experiments will then be possible: if Elliott-Yafet-type scattering (as suggested by Koopmans[2]) or exchange scattering[29] is dominating the spin-flip dynamics on different time scales (<100 fs and above) can be tested by varying the spin-orbit interaction, promoting Elliott-Yafet-type interaction on one side or studying materials with an increased value of the exchange splitting, promoting the second type.

ACKNOWLEDGMENTS

The authors would like to acknowledge A. Kimel for valuable discussions and a critical reading of the manuscript, and from the Spanish Ministry of Science and Innovation through the grants MAT2007-66719-C03-01 and CS2008-023, and the German Research Foundation within SPP 1133.

[1] E. Beaurepaire, J. C. Merle, A. Daunois, and J. Y. Bigot, Phys. Rev. Lett. **76**, 4250 (1996).

[2] B. Koopmans, in *Spin Dynamics in Confined Magnetic Structures II*, edited by B. Hillebrands and K. Ounadjela (Springer-Verlag, Berlin, 2003).

[3] B. Koopmans, J. J. M. Ruigrok, F. Dalla Longa, and W. J. M. de Jonge, Phys. Rev. Lett. **95**, 267207 (2005).

[4] F. Hansteen, A. Kimel, A. Kirilyuk, and T. Rasing, Phys. Rev. Lett. **95**, 047402 (2005).

[5] C. Stamm, T. Kachel, N. Pontius, R. Mitzner, T. Quast, K. Holldack, S. Khan, C. Lupulescu, E. F. Aziz, M. Wietstruk, H. A. Dürr, and W. Eberhardt, Nature Mater. **6**, 740 (2007).

[6] M. Cinchetti, M. Sánchez Albaneda, D. Hoffmann, T. Roth, J.-P. Wüstenberg, M. Krausss, O. Andreyev, H. C. Schneider, M. Bauer, and M. Aeschlimann, Phys. Rev. Lett. **97**, 177201 (2006).

[7] I. Radu, G. Woltersdorf, M. Kiessling, A. Melnikov, U. Bovensiepen, J.-U. Thiele, and C. H. Back, Phys. Rev. Lett. **102**, 117201 (2009); A. Melnikov, H. Prima-Garcia, M. Lisowski, T. Gießel, R. Weber, R. Schmidt, C. Gahl, N. M. Bulgakova, U. Bovensiepen, and M. Weinelt, *ibid.* **100**, 107202 (2008).

[8] J.-Y. Bigot, M. Vomir, and E. Beaurepaire, Nat. Phys. **5**, 515 (2009).

[9] E. Carpene, E. Mancini, C. Dallera, M. Brenna, E. Puppin, and S. De Silvestri, Phys. Rev. B **78**, 174422 (2008).

[10] G. M. Müller, M. Djordjevic, G.-X. Miao, A. Gupta, A. V. Ra-

mos, K. Gehrke, V. Moshnyaga, K. Samwer, J. Schmalhorst, A. Thomas, A. Hütten, G. Reiss, J. S. Moodera, and M. Münzenberg, Nature Mater. **8**, 56 (2009).
[11] J. Walowski, G. Müller, M. Djordjevic, M. Münzenberg, M. Kläui, C. A. F. Vaz, and J. A. C. Bland, Phys. Rev. Lett. **101**, 237401 (2008).
[12] F. Dalla Longa, J. T. Kohlhepp, W. J. M. de Jonge, and B. Koopmans, Phys. Rev. B **75**, 224431 (2007).
[13] G. P. Zhang and W. Hübner, Phys. Rev. Lett. **85**, 3025 (2000).
[14] A. V. Kimel, A. Kirilyuk, P. A. Usachev, R. V. Pisarev, A. M. Balbashov, and Th. Rasing, Nature (London) **435**, 655 (2005).
[15] A. Rebei and J. Hohlfeld, Phys. Lett. A **372**, 1915 (2008).
[16] N. Kazantseva, U. Nowak, R. W. Chantrell, J. Hohlfeld, and A. Rebei, EPL **81**, 27004 (2008); N. Kazantseva, D. Hinzke, U. Nowak, R. W. Chantrell, and O. Chubykalo-Fesenko, Phys. Status Solidi **244**, 4389 (2007).
[17] N. Kazantseva, D. Hinzke, U. Nowak, R. W. Chantrell, U. Atxitia, and O. Chubykalo-Fesenko, Phys. Rev. B **77**, 184428 (2008).
[18] J. Hohlfeld, S. S. Wellershoff, J. Güdde, U. Conrad, V. Jähnke, and E. Matthias, Chem. Phys. **251**, 237 (2000).
[19] M. I. Kaganov, I. M. Lifshitz, and L. V. Tanatarov, Sov. Phys. JETP **4**, 173 (1957).
[20] R. W. Schoenlein, W. Z. Lin, J. G. Fujimoto, and G. L. Eesley, Phys. Rev. Lett. **58**, 1680 (1987).
[21] P. B. Allen, Phys. Rev. Lett. **59**, 1460 (1987).
[22] M. Djordjevic and M. Münzenberg, Phys. Rev. B **75**, 012404 (2007); J. Walowski, M. Djordjevic Kaufmann, B. Lenk, C. Hamann, J. McCord, and M. Münzenberg, J. Phys. D **41**, 164016 (2008).
[23] B. Koopmans, G. Malinowski, F. Dalla Longa, D. Steiauf, M. Fähnle, T. Roth, M. Cinchetti, and M. Aeschlimann, Nature Mater. **9**, 259 (2010).
[24] U. Atxitia, O. Chubykalo-Fesenko, N. Kazantseva, D. Hinzke, U. Nowak, and R. W. Chantrell, Appl. Phys. Lett. **91**, 232507 (2007).
[25] R. J. Elliott, Phys. Rev. **96**, 266 (1954); Y. Yafet, Solid State Phys. **14**, 1 (1963).
[26] D. Steiauf, and M. Fähnle, Phys. Rev. B **79**, 140401(R) (2009).
[27] M. Krauß, T. Roth, S. Alebrand, D. Steil, M. Cinchetti, M. Aeschlimann, and H. C. Schneider, Phys. Rev. B **80**, 180407(R) (2009).
[28] By taking into account the correct matrix elements in the scattering process, angular momentum conservation is fulfilled. We assume that the possibility to couple to a phonon in such a scattering event is always given, mediated by spin-orbit interaction somehow (e.g., the dispersion of two transverse polarized branches along high-symmetry directions are equal, which allows to form a circularly polarized phonon branch). Quantitative calculations are currently performed by M. Fähnle and his group and not available yet.
[29] J. Hong and D. L. Mills, Phys. Rev. B **62**, 5589 (2000).
[30] T. Balashov, A. F. Takács, M. Däne, A. Ernst, P. Bruno, and W. Wulfhekel, Phys. Rev. B **78**, 174404 (2008).
[31] M. Plihal, D. L. Mills, and J. Kirschner, Phys. Rev. Lett. **82**, 2579 (1999).
[32] D. M. Edwards and F. A. Hertz, J. Phys. F: Met. Phys. **3**, 2191 (1973).
[33] H. A. Mook and R. M. Nicklow, Phys. Rev. B **7**, 336 (1973); H. A. Mook, R. M. Nicklow, E. D. Thompson, and M. K. Wilkinson, J. Appl. Phys. **40**, 1450 (1969).
[34] J. F. Cooke, J. W. Lynn, and H. L. Davis, Phys. Rev. B **21**, 4118 (1980).
[35] M. Djordjevic, M. Lüttich, P. Moschkau, P. Guderian, T. Kampfrath, R. G. Ulbrich, M. Münzenberg, W. Felsch, and J. S. Moodera, Phys. Status Solidi C **3**, 1347 (2006).
[36] D. A. Garanin, Phys. Rev. B **55**, 3050 (1997); Physica A **172**, 470 (1991).
[37] O. Chubykalo-Fesenko, U. Nowak, R. W. Chantrell, and D. Garanin, Phys. Rev. B **74**, 094436 (2006).
[38] M. Braun, R. Kohlhaas, and O. Vollmer, Z. Angew. Phys. **25**, 365 (1968).
[39] A. P. Caffrey, P. E. Hopkins, J. M. Klopf, and P. M. Norris, Microscale Thermophys. Eng. **9**, 365 (2005).
[40] For long time scales the at ≈ 20 ps the temperature of the magnetic system T_s is determined from the Langevin function by the decrease in magnetization. For this delay time the electron temperature is set to $T_e = T_s$. At negative delay T_e and T_s are assumed to be at room temperature again which is fulfilled in good approximation and we set $T_e = T_s = 300$ K. By this procedure the deposited energy per pulse $P(t)$ within the 15 nm Ni layer can be adjusted. See also supplementary materials section.
[41] K. Chen and D. P. Landau, Phys. Rev. B **49**, 3266 (1994).
[42] K. Gilmore, Y. U. Idzerda, and M. D. Stiles, Phys. Rev. Lett. **99**, 027204 (2007).
[43] J. Kuneš and V. Kambersky, Phys. Rev. B **65**, 212411 (2002).
[44] See supplementary material at http://link.aps.org/supplemental/10.1103/PhysRevB.81.174401 for additional technical details and information on the analysis procedure.